ORIGINAL ARTICLE

JBMR®

A Novel *IFITM5* Mutation in Severe Atypical Osteogenesis Imperfecta Type VI Impairs Osteoblast Production of Pigment Epithelium-Derived Factor

Charles R Farber,[1,2]* Adi Reich,[3]* Aileen M Barnes,[3] Patricia Becerra,[4] Frank Rauch,[5,6] Wayne A Cabral,[3] Alison Bae,[3] Aaron Quinlan,[1,2] Francis H Glorieux,[5,6] Thomas L Clemens,[7,8] and Joan C Marini[3]

[1]Center for Public Health Genomics, University of Virginia, Charlottesville, VA, USA
[2]Departments of Public Health Sciences, Biochemistry, and Molecular Genetics, University of Virginia, Charlottesville, VA, USA
[3]Bone and Extracellular Matrix Branch, NICHD, NIH, Bethesda, MD, USA
[4]Section on Protein Structure and Function, LRCMB, NEI, NIH, Bethesda, MD, USA
[5]Shriners Hospital for Children, Montreal, Canada
[6]McGill University, Montreal, Canada
[7]Department of Orthopaedic Surgery, Johns Hopkins School of Medicine, Baltimore, MD, USA
[8]Baltimore VA Medical Center, Baltimore, MD, USA

ABSTRACT

Osteogenesis imperfecta (OI) types V and VI are caused, respectively, by a unique dominant mutation in *IFITM5*, encoding BRIL, a transmembrane ifitm-like protein most strongly expressed in the skeletal system, and recessive null mutations in *SERPINF1*, encoding pigment epithelium-derived factor (PEDF). We identified a 25-year-old woman with severe OI whose dermal fibroblasts and cultured osteoblasts displayed minimal secretion of PEDF, but whose serum PEDF level was in the normal range. *SERPINF1* sequences were normal despite bone histomorphometry consistent with type VI OI and elevated childhood serum alkaline phosphatase. We performed exome sequencing on the proband, both parents, and an unaffected sibling. *IFITM5* emerged as the candidate gene from bioinformatics analysis, and was corroborated by membership in a murine bone co-expression network module containing all currently known OI genes. The de novo *IFITM5* mutation was confirmed in one allele of the proband, resulting in a p.S40L substitution in the intracellular domain of BRIL but was absent in unaffected family members. *IFITM5* expression was normal in proband fibroblasts and osteoblasts, and BRIL protein level was similar to control in differentiated proband osteoblasts on Western blot and in permeabilized mutant osteoblasts by microscopy. In contrast, *SERPINF1* expression was decreased in proband osteoblasts; PEDF was barely detectable in conditioned media of proband cells. Expression and secretion of type I collagen was similarly decreased in proband osteoblasts; the expression pattern of several osteoblast markers largely overlapped reported values from cells with a primary PEDF defect. In contrast, osteoblasts from a typical case of type V OI, with an activating mutation at the 5′-terminus of BRIL, have increased *SERPINF1* expression and PEDF secretion during osteoblast differentiation. Together, these data suggest that BRIL and PEDF have a relationship that connects the genes for types V and VI OI and their roles in bone mineralization. © 2014 American Society for Bone and Mineral Research.

KEY WORDS: *IFITM5*; BRIL; *SERPINF1*; PEDF; OSTEOGENESIS IMPERFECTA; OI

Introduction

Osteogenesis imperfecta (OI), also known as "brittle bone disease," is a heritable bone dysplasia characterized by susceptibility to fracture from minor trauma, growth deficiency, and varying associated connective tissue findings.[1,2] The etiology of OI is collagen associated: Defects in the genes encoding type I collagen, *COL1A1* and *COL1A2*, cause autosomal dominant OI and are responsible for the great majority of cases,[3] whereas defects in genes whose products interact with collagen for chaperoning, post-translational modification, folding, isomerization, or crosslinking result in autosomal recessive or dominant forms of OI.[1]

Types V and VI OI, first clinically delineated in 2000 and 2002, respectively, are each characterized by distinct defects in bone mineralization.[4,5] Patients with type V OI have dominant

Received in original form September 9, 2013; revised form December 9, 2013; accepted January 1, 2014. Accepted manuscript online January 13, 2014.
Address correspondence to: Joan C Marini, MD, PhD, Chief, Bone and Extracellular Matrix Branch, NICHD, NIH, Building 10: Room 10D39, 9000 Rockville Pike, Bethesda, MD 20892, USA. E-mail: oidoc@helix.nih.gov
*The first two authors contributed equally to this work.
Presented in part as a Late Breaking Platform Presentation at the 2012 ASBMR Meeting; October 12–15, 2012; Minneapolis, MN.
Additional Supporting Information may be found in the online version of this article.

Journal of Bone and Mineral Research, Vol. 29, No. 6, June 2014, pp 1402–1411
DOI: 10.1002/jbmr.2173

inheritance of moderately severe bone dysplasia and fracture incidence, including vertebral compressions and often scoliosis. They do not have blue sclerae or dentinogenesis imperfecta. Distinctive features of type V OI include radial head dislocation (86% of cases), ossification of the forearm interosseous membrane (95% of cases), and hyperplastic callus (65% of cases). There is also a radiographically dense band that is prominent in the forearm metaphyses. The combination of features present in any given patient is variable, as is the timing of appearance: The dense metaphyseal band appears in infancy, interosseous membrane calcification generally appears before age 2 years, radial head dislocation as early as 3.5 years of age, and hyperplastic callus by the teen years.[5,6] All patients with type V OI have a distinctive meshlike lamellation pattern on bone histology.[7]

The clinical characteristics and bone histomorphometry of patients with type VI OI are distinct from type V.[5] Patients with type VI have recessive inheritance of bone dysplasia. They do not have fractures at birth but subsequently have more frequent fractures (more than 10 per year) that progressively lead to bone deformity. All have vertebral compressions and most have scoliosis. Growth deficiency in type VI is moderately severe, sclerae are white, and teeth are normal. Children with type VI OI have elevated serum alkaline phosphatase levels, with a mean of 409 U/L (range 200 to 650 U/L).[5] Their iliac crest histology is remarkable for broad bands of unmineralized osteoid and a fish-scale pattern under polarized light; the mineralization lag time is significantly prolonged on quantitative histomorphometry.[5,7,8]

Recently, the genes responsible for types V and VI OI have been delineated. All cases of type V OI are caused by a recurrent heterozygous mutation in the 5′-UTR of *IFITM5* (c.-14C > T).[9–11] *IFITM5* encodes BRIL, a transmembrane protein enriched in osteoblasts during mineralization.[12,13] The type V OI mutation putatively adds 5 amino acids to the N-terminus of BRIL and may cause a gain-of-function with respect to extracellular BRIL ligands. The causative gene for type VI OI is *SERPINF1*, which encodes pigment epithelium-derived factor (PEDF); a number of null recessive mutations have been reported.[8,14–16] PEDF is a ubiquitously expressed secreted protein with multiple functions. It is a potent anti-angiogenic factor that inhibits tumor growth and metastasis, a neurotropic and anti-apoptotic factor, as well as being implicated in lipid metabolism.[17–20] Serum PEDF is <0.3 ng/L in type VI OI patients, whereas normal PEDF values are reported in type V OI, as well as in OI caused directly by collagen defects (types I, III, and IV).[8] PEDF and BRIL are not known to interact in any way.

Recently, we investigated the etiology of extremely severe OI in a young adult who had many of the characteristics of type VI but lacked crucial features. We used exome sequencing and a bone co-expression network analysis to identify a causative mutation in *IFITM5*, distinct from the mutation causing type V OI. Our investigations into the mechanism of OI in this individual implicate an association between BRIL and secretion of PEDF.

Materials and Methods

Mutation identification and verification

We screened genomic DNA (gDNA) of dermal fibroblasts, leukocytes, or both from the proband as well as from her parents and unaffected sibling. Sequencing of complementary DNA (cDNA) and gDNA from the proband revealed no mutations in *COL1A1, COL1A2, CRTAP, LEPRE1, PPIB, SERPINH1, FKBP10*, or *SERPINF1*. The mutation in *IFITM5* that causes type V OI had not been reported when our investigation began. All patient skin and bone biopsies were obtained with informed consent under a protocol approved by the NICHD IRB.

After exome sequencing was analyzed, the two exons and flanking intronic sequences of *IFITM5* gDNA from leukocytes of control, proband, sibling, and parents were amplified by PCR, as previously described,[9] and sequenced. Proband and control *IFITM5* cDNA from fibroblasts was also sequenced.

Exome sequencing

Exome sequencing was performed by the Genomic Services Lab at the HudsonAlpha Institute for Biotechnology (Huntsville, AL, USA). Briefly, gDNA (1 to 2 μg) was fragmented and subjected to exome enrichment using the Nimblegen SeqCap EZ Human Exome Library v2.0 kit (Roche Nimblegen, Madison, WI, USA). The enriched libraries were barcoded and 100-bp paired-end reads were generated on an Illumina HiSeq2000 (Illumina, San Diego, CA, USA).

The raw sequencing reads in FASTQ format were aligned to the UCSC hg19 human genome sequence using the Burrows-Wheeler Aligner (BWA).[21] On-target read pairs (located ± 500 bp of an exon target) with mapping qualities ≥20 were identified using the SAMtools[22] and BEDTools utilities.[23] Duplicate reads were flagged using the Picard MarkDuplicates utility (http://picard.sourceforge.net/). Realignment of sequence surrounding insertions/deletions (Indels) and base quality score recalibration was accomplished with the Genome Analysis Toolkit (GATK).[24] The GATK Unified Genotyper was used to call single nucleotide variants (SNVs) and Indels. Variants with Phred scaled quality scores ≤30 were excluded. Variants were functionally annotated using SNPEff v2.0.5[25] and ANNOVAR.[26] Filtering of variants was done using a custom R script. Putatively causal variants were manually inspected using the Integrated Genomics Viewer.[27,28]

Weighted Gene Co-expression Network Analysis (WGCNA)

The methods used to generate the Weighted Gene Co-expression Network used in this study are provided by Calabrese and colleagues.[29] Briefly, the WGCNA algorithm[30] was applied to bone microarray gene expression data from 96 inbred strains from the Hybrid Mouse Diversity Panel (available from the NCBI Gene Expression Omnibus (GSE27483)).[31,32] We first calculated Pearson correlation coefficients for all gene-gene comparisons across all microarray samples. The matrix of correlations was then converted to an adjacency matrix of gene-gene relationships. The adjacencies were defined as $\alpha_{ij} = |cor(x_i, x_j)|^{\beta}$ where x_i and x_j are the i^{th} and j^{th} gene expression traits. The power $\beta = 8$ was selected using the scale-free topology criterion outlined by Zhang and Horvath.[33] The topological overlap measure (TOM) between the i^{th} and j^{th} gene expression traits was then measured as $TOM = \frac{\sum_{u \neq i,j} a_{iu}a_{uj} + a_{ij}}{\min(k.total_i, k.total_j) + 1 - a_{ij}}$, where $\sum_{u \neq i,j} a_{iu}a_{uj}$ denotes the number of nodes to which both i and j are connected, and u indexes the nodes of the network. A TOM-based dissimilarity measure ($1 - TOM$) was used for hierarchical clustering. Gene modules corresponded to the branches of the resulting dendrogram and were precisely defined using the "Dynamic Hybrid" branch cutting algorithm.[34] In this network, the strength of gene-gene connections are quantified by the TOM.

Cell culture

Dermal fibroblast (FB) cultures were established from skin punch biopsies. FB were grown in Dulbecco's Modified Eagle Medium (DMEM) containing 10% fetal bovine serum (FBS), 100 U/mL penicillin, and 100 μg/mL streptomycin. Osteoblast (OB) primary cultures were established from surgical bone chips.[35] OB were cultured in MEM alpha (Life Technologies, Grand Island, NY, USA) supplemented with 10% FBS, penicillin, and streptomycin at 37°C and 8% CO_2. Osteoblast cultures were grown to confluence, then treated with osteoblast differentiation medium (containing 25 μg/mL L-ascorbic acid, Dexamethasone (10^{-8}M), and 2.5 mM 2-glycerophosphate, with or without 100 ng/mL BMP2).

RT-PCR

Total RNA was extracted from control and proband primary osteoblast and fibroblast cultures using TriReagent (Molecular Research Center, Cincinnati, OH, USA). cDNA was reversed transcribed from 5 μg RNA using a High-Capacity cDNA Archive Kit or MuLV reverse transcriptase and Oligo $d(T)_{16}$ (Life Technologies). Transcript levels of *IFITM5, SERPINF1, COL1A1, ALPL, BGLAP, SPP1*, and *IBSP* (Life Technologies) were determined with Taqman Gene Expression Assays. Relative expression of each gene of interest was compared with expression of *GAPDH*. Expression levels were normalized to age-matched control osteoblasts (day 1). Expression of *IFITM5* in osteoblasts and fibroblasts by PCR as shown in Fig. 3*A* used primers in exon 1 (F: 5′-TTGATCTGGTCGGTGTTCAG-3′) and exon 2 (5′-GTCAGTCA-TAGTCCGCGTCA-3′) as previously described[9] and generated the expected 292-bp product.

Western blot and ELISA

Cell lysates were collected in RIPA buffer supplemented with a protease inhibitor cocktail (Sigma-Aldrich, St. Louis, MO, USA). Osteoblast conditioned media was collected after incubation for 24 hours in serum-free media and supplemented with protease inhibitors. Media was concentrated using centrifugal filters (EMD Millipore, Billerica, MA, USA) and normalized to cell counts for equal loading.

Proteins were separated on precast 4% to 15% Ready Gels (Bio-Rad, Hercules, CA, USA), transferred to 0.2-μm nitrocellulose membranes, and blocked with 5% bovine serum albumin (BSA) plus 1× casein in PBS before probing with antibody overnight in 2.5% BSA and 0.5× casein. Antibodies used were as follows: IFITM5 (Abcam, Cambridge, MA, USA), COL1A1 LF-68 (the generous gift of Dr Larry W Fisher), PEDF (EMD Millipore), and actin (Sigma-Aldrich). Blots were washed, incubated with secondary IR-conjugated antibodies for 1 hour, washed, and visualized on a LI-COR Odyssey infrared imager (LI-COR, Lincoln, NE, USA).

Serum samples were collected from patient and control, divided into aliquots, and stored at −80°C. PEDF in sera was isolated from other proteins present in serum by cation-exchange column chromatography using 0.5 mL of S-Sepharose, Fast-flow resins, buffer S (20 mM Na-phosphate pH 6.5, 1 mM DTT, 5% glycerol). Load was 0.5 mL serum diluted 1:10 in buffer S. After washing the column with 20-column volumes to separate the unbound material, PEDF protein was eluted from the resin with 1.2 mL of 1 M NaCl in buffer S. PEDF protein was quantified in the eluted fractions using Human PEDF ELISA kit (BioProducts, Middletown, MD, USA).

Histology and histomorphometry

Full-thickness transiliac bone biopsy specimens were obtained with a Bordier trephine (5 mm core diameter) under general anesthesia, from a site located 2 cm below and behind the anterior superior iliac spine. Biopsy specimens were processed and analyzed as previously described.[36]

Immunofluorescence microscopy

Control and proband osteoblasts were grown to confluence on chamber slides, then treated with osteoblast differentiation medium (MEM Alpha containing 10% FBS, 25 μg/mL L-ascorbic acid, Dexamethasone [10^{-8}M], and 2.5 mM 2-glycerophosphate) for 10 days. Cells were washed in PBS, fixed in 4% paraformaldehyde, and stained as previously described.[37] Briefly, cells were permeabilized in 1% goat serum plus 0.2% Triton X-100 for 5 minutes, washed, and blocked in 1% BSA in PBS. Cells were incubated with BRIL primary antibody (Abcam ab107185, Cambridge, MA, USA) in 1% BSA in PBS. After washing, cells were incubated with secondary antibody, and then washed slides were mounted with DAPI (Vector Laboratories, Burlingame, CA, USA), and imaged using a Zeiss LSM 510 Inverted Meta microscope and LSM510 software.

Statistical analysis

The data were analyzed using repeated-measures *t* test. Values are presented as mean ± SD unless noted. Significance was achieved at $p \leq 0.05$.

Results

Proband case report

The proband is a 25-year-old white woman with extremely severe progressive OI who was followed at the NIH Clinical Center from age 4 years. She was delivered vaginally at 31 weeks gestation with frank breech presentation, as the product of a pregnancy complicated by polyhydramnios. At birth, her weight (1600 gms) was normal for gestational age, head circumference was 27.5 cm (50th centile for 29 weeks gestation), and length was 39 cm (50th centile for an infant of 26 weeks gestation). Blue sclerae and bowed limbs with multiple long bone fractures were noted in the newborn period. Transient cardiac failure was reported during the first year of life. Currently, she has mild regurgitation of the tricuspid valve but no cardiac symptoms. She had symptoms of asthma from ages 5 to 10 years. Spiral computed tomography (CT) for basilar invagination was negative at 20 years of age but detected mild stenosis of her central canal at C4. She was never able to ambulate and utilized a powered wheelchair for mobility. As a child, she was able to bear weight briefly for transfers and was active in swimming. Intellectual development is normal; the proband is now a graduate student.

She suffered multiple fractures of ribs and had 5 femur fractures before age 10 years. In childhood, her L_1 to L_4 DXA z-scores were in the -2 range; after several years of Fosamax® during her late teens, her current *z*-score = 0.4 (0.713 gm/cm^2). Radiographs showed bowed and severely dysplastic long bones by age 4 years (Supplemental Fig. S1), with a progressive increase in Erlenmeyer deformity at metaphyses and eventual resolution of radiographic "popcorn" formation[38] by adulthood (Fig. 1*A*). She developed scoliosis in preteen years. Her vertebral bodies were notable for numerous small cystic lesions, but vertebral geometry was reasonably well preserved (Fig. 1*A*). The typical

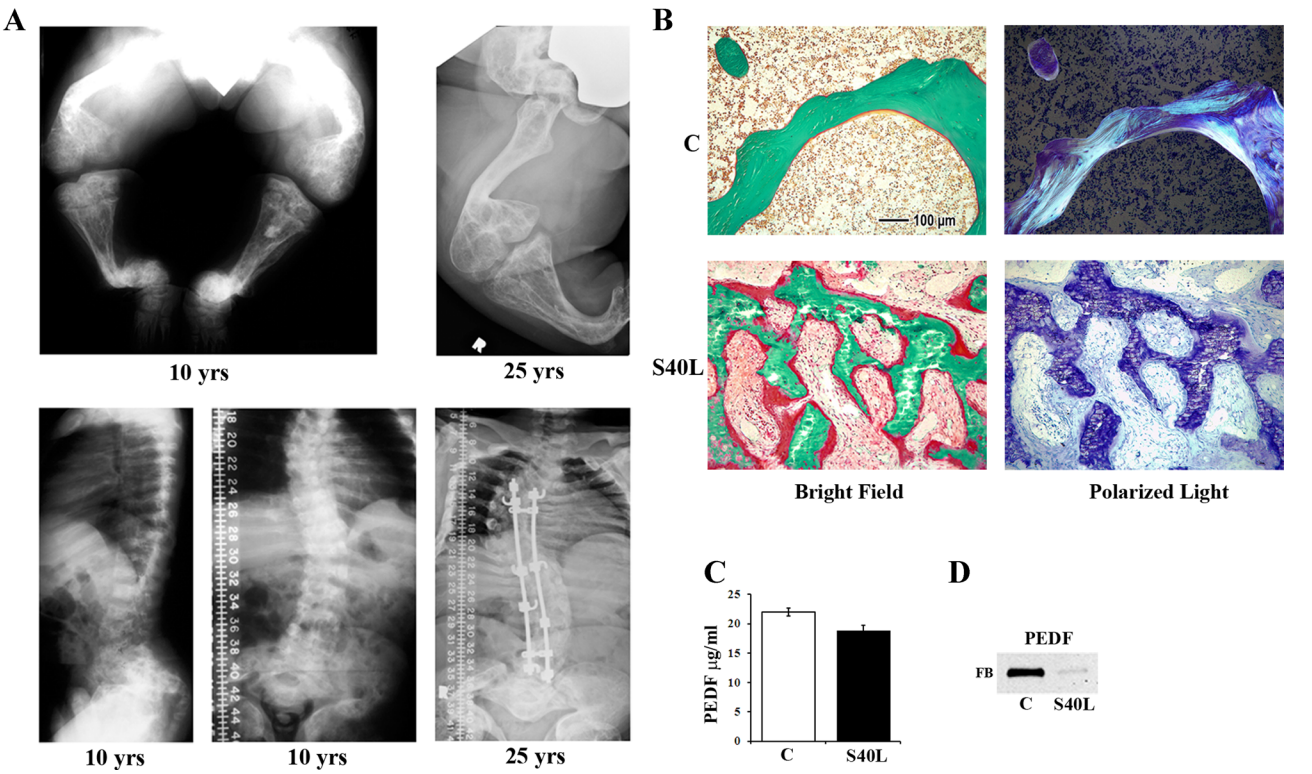

Fig. 1. (*A*) Radiographs of proband show the long bones of the lower limbs, thorax, and lateral spine at 10 and 25 years old. Radiographs show bowed and severely dysplastic long bones, with progressive increase in Erlenmeyer deformity at metaphyses and eventual resolution of radiographic "popcorn" formation by adulthood. Lower panel shows S-curve scoliosis, which has been surgically stabilized, and prominent lordosis. (*B*) Sections of iliac crest biopsy of proband (S40L) and age-matched control (C) stained with Goldner and toluidine-blue, and viewed with bright field and polarized light, respectively. Proband sample shows the accumulation of osteoid and loss of normal orientation of the lamellae, with a fish-scale pattern under polarized light. (*C*) PEDF serum concentrations in proband (S40L) and age-matched control (C) were in the normal range. (*D*) Western blot of PEDF secretion from control (C) and proband (S40L) fibroblasts (FB) show absence of PEDF secretion in proband.

features of type V OI, dense metaphyseal bands, hypertrophic callus, radial head dislocation, and ossification of the interosseous membrane,[10] were not observed.

Between ages 2 to 9 years, she required 7 rodding procedures including femora, tibias, and humerus; spine instrumentation was done at 12 years of age. Her growth has always been extremely slow; her moderate response to rGH treatment did not significantly affect her stature. In conjunction with the rGH treatment protocol, she underwent a transiliac biopsy at age 7 years, which showed broad bands of unmineralized osteoid and a fish-scale pattern of lamellation, as seen in type VI OI (Fig. 1*B*). Trabecular thickness was reduced and osteoclast surface was increased. Kinetic data could not be obtained because the tetracycline labels were blurred because of moderately severe osteomalacia (Supplemental Table S1).

From ages 6 to 8 years, her serum alkaline phosphatase was significantly elevated (964 to 1384 IU/L) but decreased to 209 IU/L at age 21 years and is now 118 IU/L at age 25 years. Also at 25 years, her BSAP is 48 µg/L and osteocalcin is 56.7 ng/mL (reference range 7.3 to 38.5 ng/mL). Importantly, serum PEDF is 18.8 µg/mL (Fig. 1*C*) versus PEDF levels in type VI OI, which are consistently $<$0.3 ng/mL.[8] However, secretion of PEDF by proband fibroblasts was barely detectable (Fig. 1*D*), and her *SERPINF1* gDNA sequences were normal. Other known OI-causing defects, including mutations in *COL1A1* and *COL1A2*, recessive OI genes, and the type V-causing *IFITM5* mutation, were ruled out by sequencing.

On physical exam at age 25 years, she has extreme short stature and relative macrocephaly. Her weight is 33.3 kg (50th centile for 10-year-old female), length is 87 cm (50th centile for a 25-month-old girl), and head circumference is 53.5 cm (25th centile for an adult). Her face is round with a high bossed forehead. There is a blue tinge to her sclerae; she also has dentinogenesis imperfecta, as well as prominent and irregular ridges on the cutting surface of the teeth. She has a barrel chest with pectus excavatum. All extremities are severely bowed. She has an S-curve scoliosis, which has been surgically stabilized, and prominent lordosis (Fig. 1*A*). Excess skin laxity was not noted.

Gene identification by exome sequencing and co-expression network analysis

Exome sequencing was undertaken on the proband, her unaffected parents, and sibling. A total of 22.9 Gbp of exonic sequence was generated on the four family members (Supplemental Table S2). The average sample coverage ranged from 109.7X to 149.6X. More than 96% of the target exons were covered by 10 or more reads. A total of 22,407 single-nucleotide variants (SNVs) and Indels with quality scores $\geq$30 were

identified across the four exomes. Variants that were potentially causal were identified using four filters. First, we eliminated intergenic, intronic (with the exception of splice sites), noncoding, and synonymous coding variants. Next, we identified variants with familial genotype patterns consistent with a recessive or compound heterozygous mode of inheritance or putative de novo variants observed only in the proband. Variants with an allele frequency >1% in the NHLBI Exome Sequence Project were also discarded. Lastly, we manually inspected each variant in the Integrated Genomic Viewer. After filtering, 18 variants (5 recessive and 13 de novo) met these criteria (Supplemental Table S3). Five of the 18 variants were known single-nucleotide polymorphisms (SNPs); 12 other variants were of low quality and did not confirm on direct sequencing in the proband, which yielded *IFITM5* as the candidate gene.

Since a recurrent mutation in *IFITM5* had not yet been reported as the cause of type V OI, we corroborated *IFITM5* as the likely causal gene using a network-based approach. Given the proband's histomorphometry and minimal fibroblast PEDF secretion (Fig. 1*D*), it is likely that the mutant gene is in the same pathway and/or interacts with PEDF. It has been shown that genes whose proteins interact are also often highly co-expressed;[39] therefore, we hypothesized that *SERPINF1* would be connected with the causal gene in a bone co-expression network.[29] Interestingly, 9 of the 10 known OI genes (*Ppib* was the only exception and was excluded because of a poorly performing microarray probe) are members of network module 9 (M9). The probability that M9 contained 9 known OI genes just by chance is $p < 1.0 \times 10^{-6}$. Of the 18 putative candidates, *Ifitm5* was the only member of M9. *Ifitm5* was connected (TOM > 0.05) to all the 9 other known OI genes. Of all M9 genes, *Ifitm5* was the tenth most strongly connected (TOM = 0.072) to *Serpinf1* (Fig. 2*A*).

IFITM5 mutation confirmation

The *IFITM5* mutation (c.119C > T; p.S40L) is located at 299,372 bp on Chr. 11 in the hg19.[9] The C to T transition leads to a p.S40L substitution in BRIL (Fig. 2*B*). Sanger sequencing confirmed the de novo mutation in the proband and its absence in both parents and the unaffected sibling (Fig. 2*C*). The S40 residue of BRIL is conserved from humans to zebrafish[13] (Fig. 2*D*). PolyPhen-2 predicted that the variant is deleterious to BRIL protein function. Together, these data suggest that this heterozygous *IFITM5* mutation is responsible for OI in the proband. Our analysis was strengthened by the simultaneous reporting of a different dominant *IFITM5* mutation as the cause of type V OI.

Effect of the S40L mutation on *IFITM5* expression and BRIL stability

Although *IFITM5* expression is strongest in bone tissue and osteoblasts, low-level expression has been reported in fibroblast lineage cells.[40] We confirmed a low level of *IFITM5* expression in control fibroblasts (Fig. 3*A*). *IFITM5* expression is equivalent to control in cultured proband fibroblasts and osteoblasts (Fig. 3*A*), and also in proband osteoblasts differentiated for 10 days in culture (Fig. 3*B*). BRIL protein level in proband osteoblasts and fibroblasts are each similar to control when analyzed by Western blot. Although BRIL appears to be at a similar level in fibroblasts and osteoblasts, the osteoblast sample was collected at day 10 of differentiation, past the peak of BRIL expression. The peak BRIL expression in osteoblasts would be expected to be higher than the level found in cultured fibroblasts (Fig. 3*C*). In addition, detection of BRIL in permeabilized osteoblasts (Fig. 3*D*) was similar in proband versus control osteoblasts. These data suggest that the c.119C>T mutation has minimal effects on *IFITM5* expression and protein level.

Effect of BRIL S40L on PEDF and type I collagen

In osteoblasts with BRIL S40L, *SERPINF1* expression is decreased to half of control on day 10 of differentiation in culture and to about one-quarter of control levels on day 15 (Fig. 4*A*). Secreted PEDF is barely detectable in conditioned media of proband osteoblasts, as was noted in the original fibroblast observation (Fig. 4*B*).

Interestingly, *COL1A1* expression and protein secretion follow the same pattern as PEDF. *COL1A1* expression from osteoblasts with BRIL S40L is about one-fifth of control (Fig. 4*C*), and presence of the proα1(I) chain of collagen in conditioned media is minimal (Fig. 4*D*).

Effect of BRIL S40L on osteoblast differentiation

To determine whether expression of genes other than *SERPINF1* and *COL1A1* were affected by the BRIL S40L mutation, we assayed expression of several markers in proband osteoblasts on day 10 of differentiation in culture (Fig. 5). Alkaline phosphatase (*ALPL*) and osteocalcin (*BGLAP*) expression were significantly reduced in mutant osteoblasts to less than half of control values (Fig. 5*A, B*). Conversely, expression of osteopontin (*SPP1*) and bone sialoprotein (*IBSP*), both involved in bone mineralization,[41,42] was dramatically increased to 7-fold and 24-fold higher expression, respectively, than in control osteoblasts (Fig. 5*C, D*).

PEDF expression in osteoblasts from proband with type V OI

Studies with osteoblasts from a patient with type V OI further support an effect of *IFITM5* mutations on PEDF expression and secretion. During a differentiation assay of osteoblasts with the type V OI *IFITM5* mutation, expression of *SERPINF1* is increased at least twofold versus control osteoblasts from days 5 through 15 (Fig. 6*A*), with a consequent increase in secreted PEDF on days 15 and 21 of differentiation (Fig. 6*B*).

Discussion

We report here a unique proband with severe osteogenesis imperfecta, whose causative mutation connects types V and VI OI and points to an effect of BRIL on PEDF expression and secretion. The 25-year-old woman has phenotypic and bone histology findings most consistent with type VI OI, a recessive form shown in 2011 to be caused by null mutations in *SERPINF1*.[14,15] However, the patient's *SERPINF1* gene sequence is normal as is her serum PEDF, leading us to hypothesize that this patient's OI was caused by a defect in a gene whose product interacted with PEDF in fibroblasts and osteoblasts. Exome sequencing and co-expression network analysis led to a heterozygous de novo mutation in *IFITM5* (c.119C>T), causing an S40L substitution in the bone-enriched protein BRIL.[13] The identification of the proband's substitution in BRIL occurred simultaneously with multiple reports in the literature of a recurrent heterozygous *IFITM5* mutation (c.-14C>T) that caused type V OI, putatively by adding 5 amino acids to the N-terminus of BRIL.[9–11] Although the type V OI mutation identification added to our confidence

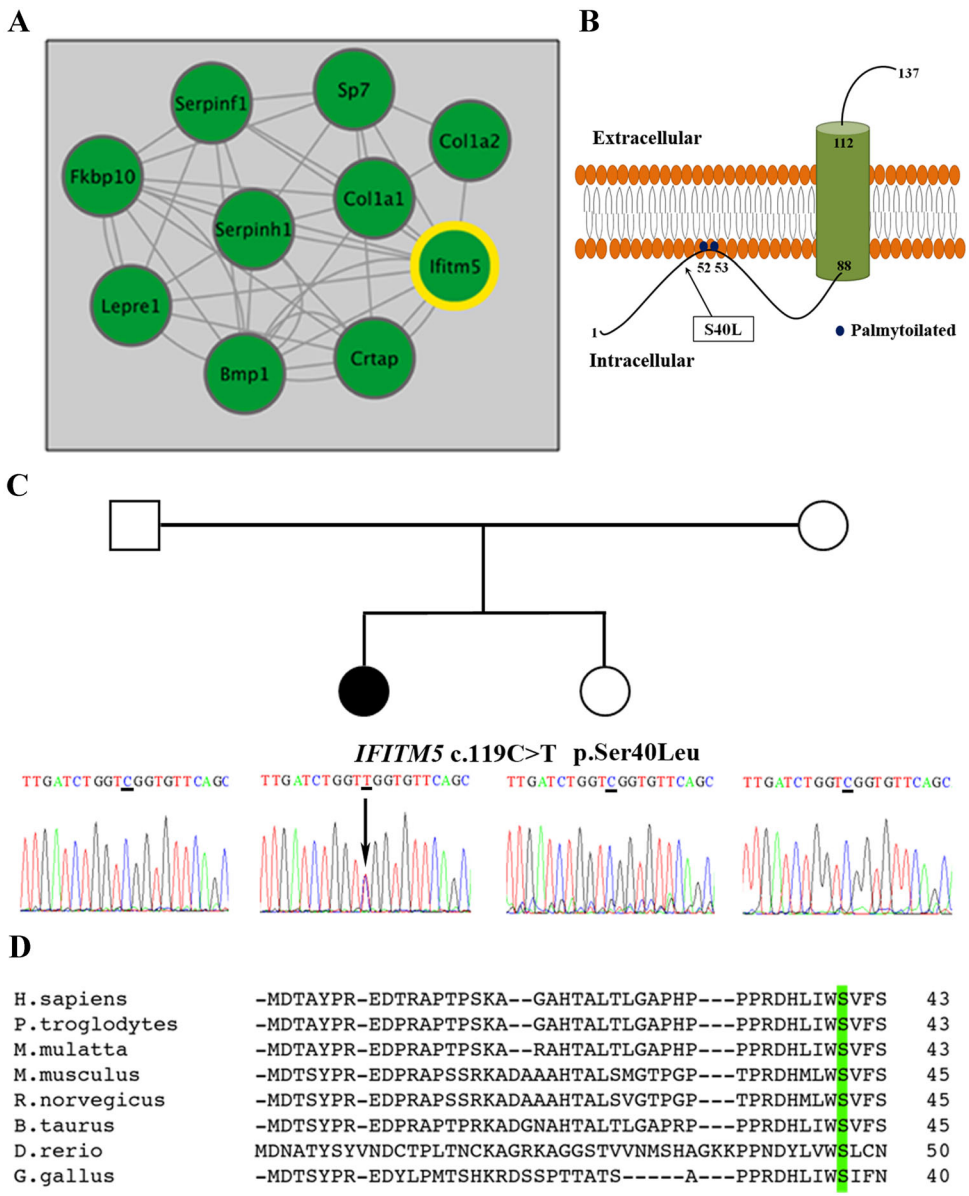

Fig. 2. (*A*) OI gene network illustrates the strong co-expression relationships between *Ifitm5* and genes known to cause OI. Each line represents a TOM > 0.05. (*B*) BRIL protein is predicted to contain one transmembrane domain, marked in green, and an intracellular domain[47]. The Ser residue substitution is marked in black on the predicted intracellular domain. (*C*) Pedigree of proband, unaffected parents, and sibling. Sanger sequencing shows the heterozygous mutation in the proband *IFITM5* gDNA. (*D*) BRIL protein sequence from various species. In all species, Ser residue in position S40 (highlighted in green) is highly conserved.

that *IFITM5* was an OI-causing gene, we also noted that our proband had none of the typical features of type V OI (dense metaphyseal bands, hypertrophic callus, radial head dislocation, and ossification of the interosseous membrane), all of which should have manifest during her prior clinical course.[4]

Our analysis identified a dominant mutation in *IFITM5* as the cause of a severe variant of type VI OI in our proband, a type typically caused by recessive null mutations of *SERPINF1*. To investigate the implied connection between PEDF and BRIL, we examined *SERPINF1* expression and PEDF secretion using cultured proband osteoblasts. *SERPINF1* expression was reduced in proband osteoblasts during differentiation, to about half on day 10 and one-quarter on day 15 of differentiation. Secretion of PEDF into conditioned media of cultured osteoblasts (day 10) was minimal, similar to fibroblast findings. We also examined the relationship of PEDF and BRIL, using osteoblasts from a patient with type V OI clinical findings and mutation. The type V OI mutation at the 5′-terminus of *IFITM5* is generally considered to be an activating mutation because patients have more active mineralization in fracture callus and the interosseus forearm membrane, and loss of function in an *Ifitm5*$^{-/-}$ mouse model[12] does not account for the human findings. The type V OI mutation results in increased expression of *SERPINF1* during osteoblast differentiation in culture when compared with the same control

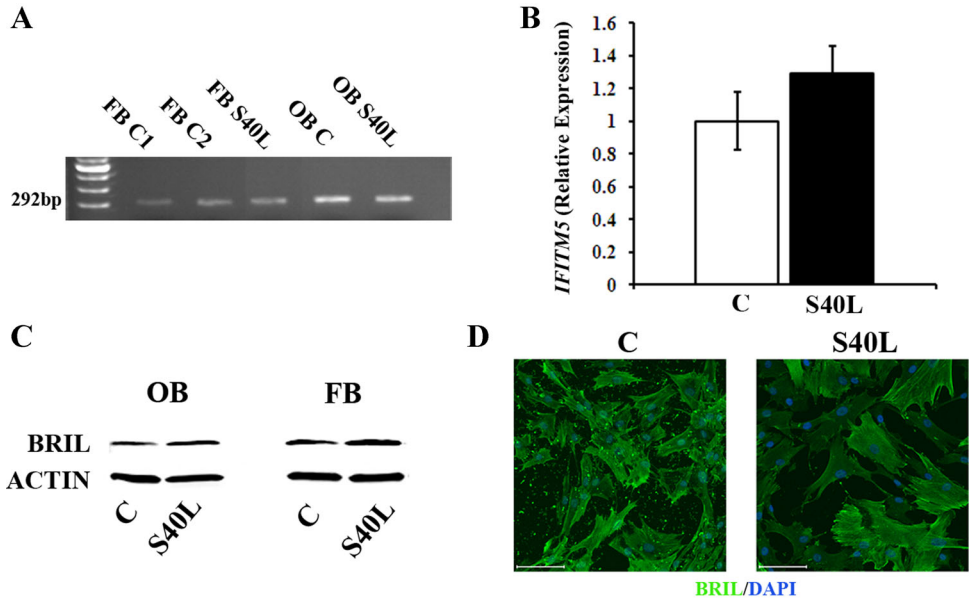

Fig. 3. (*A*) RT-PCR of cDNA detected *IFITM5* transcripts in both fibroblasts (FB) and osteoblasts (OB) from normal controls (C) and proband (S40L). (*B*) Relative *IFITM5* expression of control (C) and proband (S40L) OB stimulated with osteogenic media for 10 days with addition of BMP2 shows normal expression levels by qPCR. (*C*) Representative Western blot of BRIL protein from OB stimulated with osteogenic media for 10 days and FB showing protein stability in proband. (*D*) Immunofluorescence microscopy of permeabilized OB stimulated with osteogenic media for 10 days shows similar BRIL staining (green) in proband (S40L) and control. Scale bar = 100 μm.

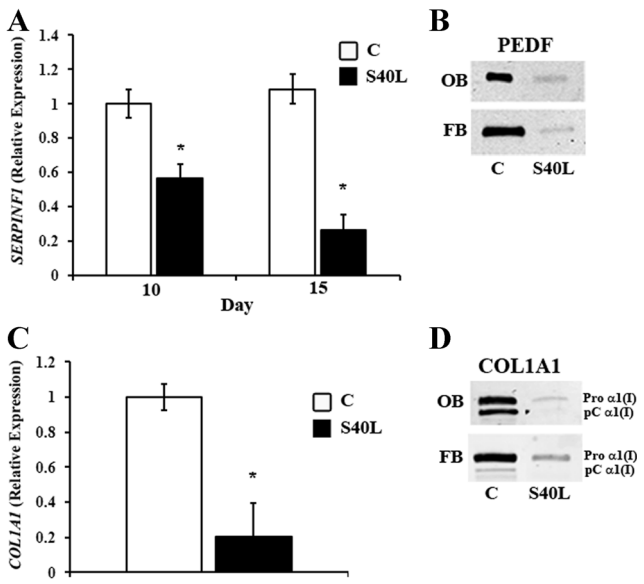

Fig. 4. (*A*) Relative *SERPINF1* expression of control (C) and proband (S40L) OB stimulated with osteogenic media for 10 and 15 days shows decreased expression in proband. (*B*) Representative Western blot from PEDF secretion of control (C) and proband (S40L) from OB stimulated with osteogenic media for 10 days and from FB. Cells show absence of PEDF secretion from proband. (*C*) Relative *COL1A1* expression of control (C) and proband (S40L) OB stimulated with osteogenic media for 10 days shows decreased expression in proband. (*D*) Representative Western blot of type I procollagen secretion from OB stimulated with osteogenic media for 10 days and from FB. Proband has minimal collagen secretion. $^{*}p < 0.05$.

cells used in studies with the atypical BRIL S40L osteoblasts. Secretion of PEDF from type V OI osteoblasts was also increased during late differentiation. *SERPINF1* expression and PEDF secretion was increased by the 5′-terminal extension in BRIL but decreased by the S40L substitution. Thus, both heterozygous BRIL defects are connected to abnormal *SERPINF1* expression and PEDF secretion.

Mutations in both *IFITM5* and *SERPINF1* have been shown to affect bone mineralization. In bone tissue of PEDF KO mice, Fourier transform-infrared (FTIR) spectroscopy shows increased mineral to matrix ratio,[43] whereas exogenous PEDF has been reported to increase mineralization by mesenchymal stem cells (MSCs) and osteoblasts in culture.[44,45] The susceptibility of classic type V OI to ectopic ossification may reflect increased local PEDF levels, just as the extreme undermineralization and bone dysplasia of the S40L case may reflect decreased local PEDF.

The reduction in *SERPINF1* expression points to a relationship between PEDF and BRIL. Attempts to demonstrate direct BRIL:PEDF binding by co-immunoprecipitation have not yielded positive results, suggesting the existence of a more complex regulatory pathway by which BRIL influences *SERPINF1* transcripts and PEDF secretion. Interestingly, type I collagen expression and secretion from BRIL S40L osteoblasts was reduced in parallel with the reduction in PEDF in those cells. These data are also consistent with the recent report that PEDF treatment increased type I collagen expression in hMSC, whereas treatment with an inhibitor of the AKT pathway reduced those transcripts.[45] Decreased collagen expression could not by itself account for the bone phenotype in our proband because type I OI patients with half-normal secretion of collagen have mild osteopenia.[46] However, decreased collagen secretion could exacerbate the PEDF-driven outcome.

An effect of BRIL on *SERPINF1* expression and PEDF secretion has not been previously reported. BRIL is a transmembrane

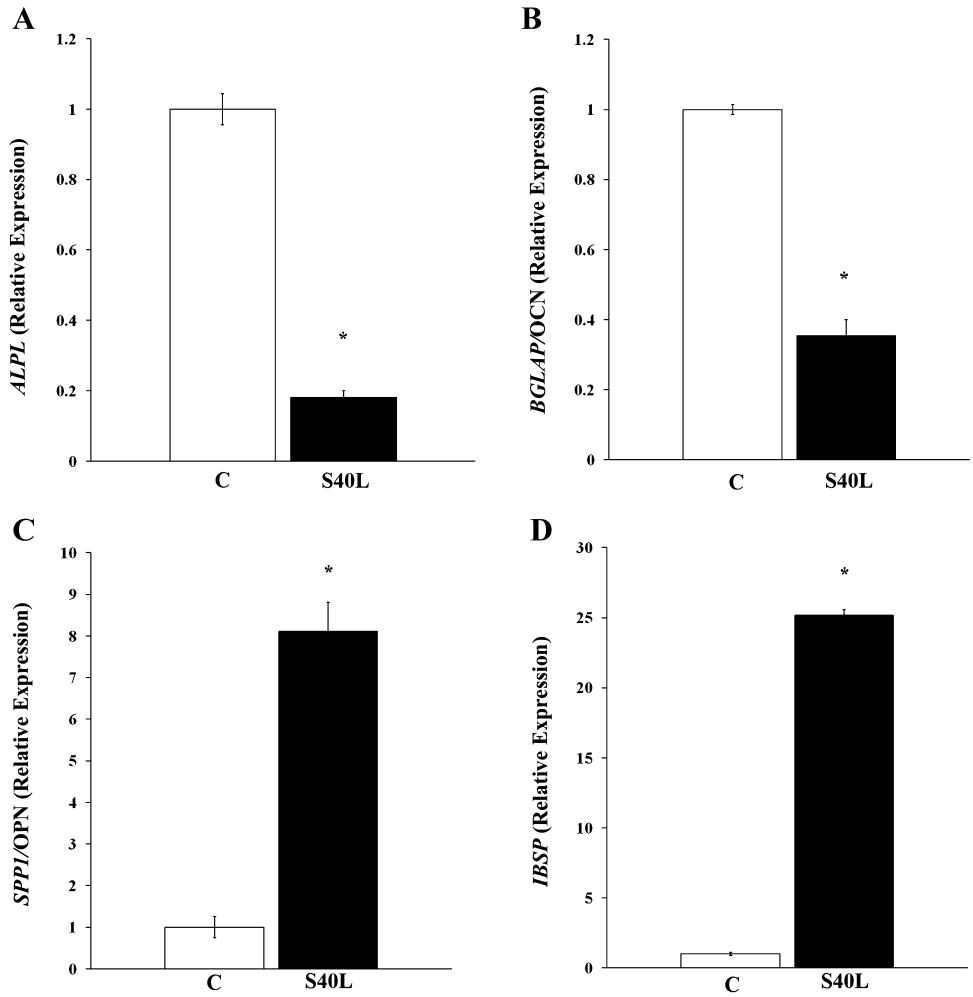

Fig. 5. (*A*) Relative alkaline phosphatase (*ALPL*) and (*B*) osteocalcin (*BGLAP*/OCN) expression in control (C) and proband (S40L) OB stimulated with osteogenic media for 10 days shows decreased expression in proband. (*C*) Relative osteopontin (*SPP1*/OPN) and (*D*) bone sialoprotein (*IBSP*) expression in control (C) and proband (S40L) OB stimulated with osteogenic media for 10 days is increased in proband. $^{*}p < 0.05$.

protein selectively enriched in osteoblasts with the N-terminus intracellular and the C-terminus extracellular.[47] During in vitro osteoblast differentiation, *IFITM5* expression coincides with mineralization.[12,13] Localization of BRIL in the plasma membrane suggests a potential for receptor function. It is not known whether the intracellular domain of BRIL is phosphorylated.[12] If BRIL is not acting as a receptor, it may serve to tether and coordinate the actions of other proteins to which it binds. The loss of the S40 residue may alter BRIL folding and interfere with the palmitoylation of BRIL residues 52 and 53[47], or with normal insertion of palmitoylated residues into the membrane.[48] Failure of mutant BRIL to insert properly in the cell membrane would likely alter BRIL interactions with other proteins. For example, BRIL has been shown to interact directly with FKBP11, an FKBP which itself is unusual for having a transmembrane domain.[12] Lack of BRIL S-palmitoylation disrupts the interaction of BRIL and FKBP11.[48] The BRIL:FKBP11 interaction was shown to occur in a larger association complex with CD81 and FPRP (prostaglandin F2 receptor negative regulator),[49] and either BRIL or FKBP11 could serve as an adaptor protein within the complex. Dissociation of CD81 from the complex leads to increased expression of multiple genes.[49] A pathway potentially regulating BRIL functioning through a membrane-associated complex is implied, and that complex could affect signaling upstream of PEDF. As in cells with a primary defect of PEDF,[44,45] proband osteoblasts have decreased expression of type I collagen, alkaline phosphatase, and osteocalcin. The increased osteopontin (*SPP1*) expression found in proband cells can be reasonably postulated to be part of the pathway by which bone mineralization is inhibited in these cells. Increased osteopontin itself contributes to decreased collagen and alkaline phosphatase levels.[41] Only bone sialoprotein (*IBSP*) expression is distinct from the pattern seen in PEDF-deficient cells because it is increased substantially in our proband but decreased in *Serpinf1* defects.[43,45] BSP plays a role in initiation of mineralization[42] and could be elevated in an abortive compensation attempt in BRIL S40L cells.

Both the S40L and 5′-extension BRIL proteins affect *SERPINF1* expression, implying that BRIL normally has a stimulatory effect on intracellular *SERPINF1* regulation. We speculate that the phenotype of our proband results from the combination of (i) its indirect effect on PEDF and (ii) direct effects of the BRIL S40L mutation itself. First, the major impact on the bone development of

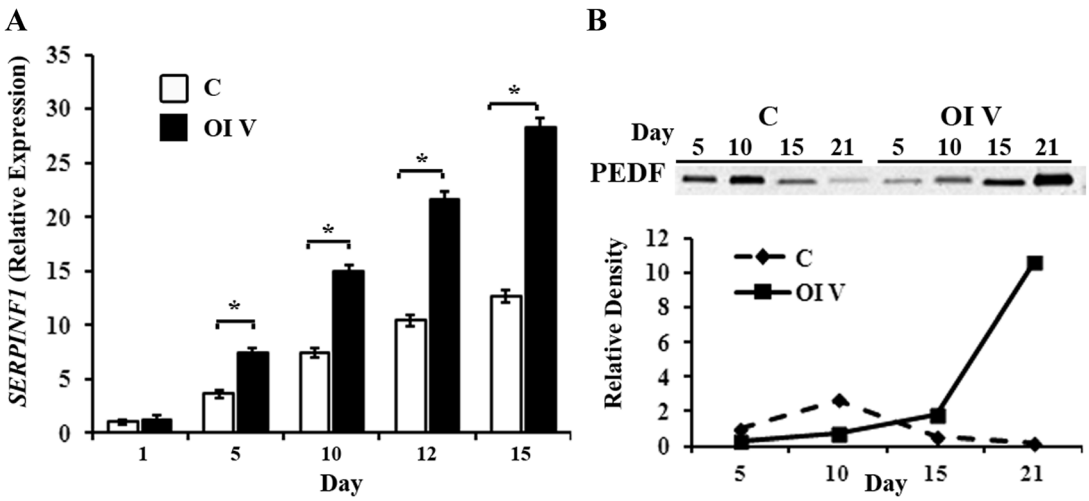

Fig. 6. (*A*) Relative *SERPINF1* transcripts in control (C) and type V OI proband (OI V). OB were cultured in osteogenic media for 1, 5, 10, or 15 days. The type V OI OB show increased *SERPINF1* expression at all time points. (*B*) Representative Western blot of PEDF secretion of OB stimulated with osteogenic media for 5, 10, 15, and 21 days. PEDF secretion was increased markedly in type V OI OB on day 21. $^{*}p < 0.05$.

the proband appears to derive from the paracrine and/or intracellular absence of PEDF. The proband's osteoblasts secrete minimally detectable levels of PEDF. Her bone histology, with broad bands of unmineralized osteoid and the characteristic fish-scale lamellation pattern under polarized light, and elevated serum alkaline phosphatase in childhood (max 1384 IU/L), even above the range reported for type VI OI (200 to 650 IU/L),[5] are compatible with type VI OI. PEDF is expressed in osteoblasts and chondrocytes and is localized primarily in areas of bone remodeling.[50] Absence of PEDF disturbs the balance between PEDF and VEGF in the matrix, negatively impacting mineralization.[51] This paracrine mechanism could be a major contribution to both *SERPINF1*-null and BRIL S40L defects, given the normal serum PEDF of the proband. Furthermore, the association of PEDF with metabolic syndrome[44] indicates intracellular functions for this protein, including a role in the plasticity of osteoblasts and adipocytes. PEDF also inhibits osteoclastogenesis,[52] thus its absence would be expected to increase bone turnover. Second, there is an apparent effect of the BRIL substitution itself because the proband's bone dysplasia has earlier onset and is radiographically and clinically more severe than the type VI OI phenotypic range. The direct BRIL effect of the S40L mutation would not be expected to contribute to ectopic mineralization because the proband has no typical type V OI findings. The essentially normal levels of BRIL in proband osteoblasts detected on Western blots and by immunofluorescence are consistent with a dominant negative dysfunction of cell: matrix interaction or signaling from cell surface to cytoplasm. Additional case reports of S40L mutations or transfection of a BRIL S40L construct into cultured osteoblasts would provide a definitive confirmation that this mutation causes the OI phenotype. Further investigation of this interesting mutation will provide insight into the functions of both proteins responsible for osteogenesis imperfecta with mineralization defects.

Disclosures

All authors state that they have no conflicts of interest.

Acknowledgments

We thank the proband and her family for their dedicated long-term support of OI research. We are grateful to Prof Pierre Moffatt for communication of unpublished results on BRIL structure in the cell membrane. We thank the NICHD Microscopy and Imaging Core in which the confocal microscopy was conducted. This work was supported by NICHD (JCM) and NEI (PB) intramural funding, extramural RO1-AR057759 (CRF), RO1-AR049410 (TLC), a VA Merit Review (TLC), and Shriners Hospital of North America (FR and FHG). FR received salary support from the Chercheur-Boursier Clinicien program of the Fonds de Recherche du Québec-Santé. TLC is also supported by a VA Senior Career Scientist Award.

Authors' roles: Study design: CRF, AR, PB, and JCM. Data collection: CRF, AR, AMB, PB, FR, WAC, and AB. Data analysis and interpretation: CRF, AR, AMB, PB, FR, WAC, AB, AQ, FHG, and JCM. Drafting manuscript: JCM, CRF, and AR. Revising manuscript content: CRF, AR, AMB, PB, FR, WAC, AB, FHG, TLC, and JCM. Approving final version of manuscript: CRF, AR, AMB, PB, FR, WAC, AB, AQ, FHG, TLC, and JCM. JCM and CRF take responsibility for the integrity of the data analysis.

References

1. Forlino A, Cabral WA, Barnes AM, Marini JC. New perspectives on osteogenesis imperfecta. Nat Rev Endocrinol. 2011;7(9):540–57.
2. Sillence DO, Senn A, Danks DM. Genetic heterogeneity in osteogenesis imperfecta. J Med Genet. 1979;16(2):101–16.
3. Marini JC, Forlino A, Cabral WA, et al. Consortium for osteogenesis imperfecta mutations in the helical domain of type I collagen: regions rich in lethal mutations align with collagen binding sites for integrins and proteoglycans. Hum Mutat. 2007;28(3):209–21.
4. Glorieux FH, Rauch F, Plotkin H, et al. Type V osteogenesis imperfecta: a new form of brittle bone disease. J Bone Miner Res. 2000;15(9):1650–8.
5. Glorieux FH, Ward LM, Rauch F, et al. Osteogenesis imperfecta type VI: a form of brittle bone disease with a mineralization defect. J Bone Miner Res. 2002;17(1):30–8.

6. Cheung MS, Glorieux FH, Rauch F. Natural history of hyperplastic callus formation in osteogenesis imperfecta type V. J Bone Miner Res. 2007;22(8):1181–6.
7. Roughley PJ, Rauch F, Glorieux FH. Osteogenesis imperfecta—clinical and molecular diversity. Eur Cell Mater. 2003;5:41–7; discussion 47.
8. Rauch F, Husseini A, Roughley P, Glorieux FH, Moffatt P. Lack of circulating pigment epithelium-derived factor is a marker of osteogenesis imperfecta type VI. J Clin Endocrinol Metab. 2012;97(8):E1550–6.
9. Cho TJ, Lee KE, Lee SK, et al. A single recurrent mutation in the 5′-UTR of IFITM5 causes osteogenesis imperfecta type V. Am J Hum Genet. 2012;91(2):343–8.
10. Rauch F, Moffatt P, Cheung M, et al. Osteogenesis imperfecta type V: marked phenotypic variability despite the presence of the IFITM5 c.-14C > T mutation in all patients. J Med Genet. 2013;50(1):21–4.
11. Semler O, Garbes L, Keupp K, et al. A mutation in the 5′-UTR of IFITM5 creates an in-frame start codon and causes autosomal-dominant osteogenesis imperfecta type V with hyperplastic callus. Am J Hum Genet. 2012;91(2):349–57.
12. Hanagata N, Li X, Morita H, et al. Characterization of the osteoblast-specific transmembrane protein IFITM5 and analysis of IFITM5-deficient mice. J Bone Miner Metab. 2011;29(3):279–90.
13. Moffatt P, Gaumond MH, Salois P, et al. Bril: a novel bone-specific modulator of mineralization. J Bone Miner Res. 2008;23(9):1497–508.
14. Becker J, Semler O, Gilissen C, et al. Exome sequencing identifies truncating mutations in human SERPINF1 in autosomal-recessive osteogenesis imperfecta. Am J Hum Genet. 2011;88(3):362–71.
15. Homan EP, Rauch F, Grafe I, et al. Mutations in SERPINF1 cause osteogenesis imperfecta type VI. J Bone Miner Res. 2011;26(12):2798–803.
16. Venturi G, Gandini A, Monti E, et al. Lack of expression of SERPINF1, the gene coding for pigment epithelium-derived factor, causes progressively deforming osteogenesis imperfecta with normal type I collagen. J Bone Miner Res. 2012;27(3):723–8.
17. Becerra SP, Notario V. The effects of PEDF on cancer biology: mechanisms of action and therapeutic potential. Nat Rev Cancer. 2013;13(4):258–71.
18. Borg ML, Andrews ZB, Duh EJ, et al. Pigment epithelium-derived factor regulates lipid metabolism via adipose triglyceride lipase. Diabetes. 2011;60(5):1458–66.
19. Dawson DW, Volpert OV, Gillis P, et al. Pigment epithelium-derived factor: a potent inhibitor of angiogenesis. Science. 1999;285(5425):245–8.
20. Filleur S, Nelius T, de Riese W, Kennedy RC. Characterization of PEDF: a multi-functional serpin family protein. J Cell Biochem. 2009;106(5):769–75.
21. Li H, Durbin R. Fast and accurate short read alignment with Burrows-Wheeler transform. Bioinformatics. 2009;25(14):1754–60.
22. Li H, Handsaker B, Wysoker A, et al. The Sequence Alignment/Map format and SAMtools. Bioinformatics. 2009;25(16):2078–9.
23. Quinlan AR, Hall IM. BEDTools: a flexible suite of utilities for comparing genomic features. Bioinformatics. 2010;26(6):841–2.
24. McKenna A, Hanna M, Banks E, et al. The Genome Analysis Toolkit: a MapReduce framework for analyzing next-generation DNA sequencing data. Genome Res. 2010;20(9):1297–303.
25. Cingolani P, Platts A, Wang Le L, et al. A program for annotating and predicting the effects of single nucleotide polymorphisms, SnpEff: SNPs in the genome of Drosophila melanogaster strain w1118; iso-2; iso-3. Fly (Austin). 2012;6(2):80–92.
26. Wang K, Li M, Hakonarson H. ANNOVAR: functional annotation of genetic variants from high-throughput sequencing data. Nucleic Acids Res. 2010;38(16):e164.
27. Robinson JT, Thorvaldsdottir H, Winckler W, et al. Integrative genomics viewer. Nat Biotechnol. 2011;29(1):24–6.
28. Thorvaldsdottir H, Robinson JT, Mesirov JP. Integrative Genomics Viewer (IGV): high-performance genomics data visualization and exploration. Brief Bioinform. 2013;14(2):178–92.
29. Calabrese G, Bennett BJ, Orozco L, et al. Systems genetic analysis of osteoblast-lineage cells. PLoS Genet. 2012;8(12):e1003150.
30. Langfelder P, Horvath S. WGCNA: an R package for weighted correlation network analysis. BMC Bioinformatics. 2008;9:559.
31. Bennett BJ, Farber CR, Orozco L, et al. A high-resolution association mapping panel for the dissection of complex traits in mice. Genome Res. 2010;20(2):281–90.
32. Farber CR, Bennett BJ, Orozco L, et al. Mouse genome-wide association and systems genetics identify Asxl2 as a regulator of bone mineral density and osteoclastogenesis. PLoS Genet. 2011;7(4):e1002038.
33. Zhang B, Horvath S. A general framework for weighted gene co-expression network analysis. Stat Appl Genet Mol Biol. 2005;4:Article17.
34. Langfelder P, Zhang B, Horvath S. Defining clusters from a hierarchical cluster tree: the Dynamic Tree Cut package for R. Bioinformatics. 2008;24(5):719–20.
35. Robey PG, Termine JD. Human bone cells in vitro. Calcif Tissue Int. 1985;37(5):453–60.
36. Glorieux FH, Travers R, Taylor A, et al. Normative data for iliac bone histomorphometry in growing children. Bone. 2000;26(2):103–9.
37. Moffatt P, Salois P, St-Amant N, Gaumond MH, Lanctot C. Identification of a conserved cluster of skin-specific genes encoding secreted proteins. Gene. 2004;334:123–31.
38. Obafemi AA, Bulas DI, Troendle J, Marini JC. Popcorn calcification in osteogenesis imperfecta: incidence, progression, and molecular correlation. Am J Med Genet A. 2008;146A(21):2725–32.
39. Vidal M, Cusick ME, Barabasi AL. Interactome networks and human disease. Cell. 2011;144(6):986–98.
40. Smith RA, Young J, Weis JJ, Weis JH. Expression of the mouse fragilis gene products in immune cells and association with receptor signaling complexes. Genes Immun. 2006;7(2):113–21.
41. Addison WN, Azari F, Sorensen ES, Kaartinen MT, McKee MD. Pyrophosphate inhibits mineralization of osteoblast cultures by binding to mineral, up-regulating osteopontin, and inhibiting alkaline phosphatase activity. J Biol Chem. 2007;282(21):15872–83.
42. Ogata Y. Bone sialoprotein and its transcriptional regulatory mechanism. J Periodontal Res. 2008;43(2):127–35.
43. Bogan R, Riddle RC, Li Z, et al. A mouse model for human osteogenesis imperfecta type VI. J Bone Miner Res. 2013;28(7):1531–6.
44. Gattu AK, Swenson ES, Iwakiri Y, et al. Determination of mesenchymal stem cell fate by pigment epithelium-derived factor (PEDF) results in increased adiposity,reduced bone mineral content. FASEB.J. 2013;27(11):4384–94.
45. Li F, Song N, Tombran-Tink J, Niyibizi C. Pigment epithelium derived factor enhances differentiation and mineral deposition of human mesenchymal stem cells. Stem Cells. 2013;31(12):2714–23.
46. Willing MC, Pruchno CJ, Atkinson M, Byers PH. Osteogenesis imperfecta type I is commonly due to a COL1A1 null allele of type I collagen. Am J Hum Genet. 1992;51(3):508–15.
47. Patoine A, Gaumond MH, Jaiswal PK, Fassier F, Rauch F, Moffatt P. Topological mapping of BRIL reveals a type II orientation and effects of osteogenesis imperfecta mutations on its cellular destination. J Bone Miner Res. 2014; doi:10.1002/jbmr.2243.
48. Tsukamoto T, Li X, Morita H, et al. Role of S-palmitoylation on IFITM5 for the interaction with FKBP11 in osteoblast cells. PLoS One. 2013;8(9):e75831.
49. Hanagata N, Li X. Osteoblast-enriched membrane protein IFITM5 regulates the association of CD9 with an FKBP11-CD81-FPRP complex and stimulates expression of interferon-induced genes. Biochem Biophys Res Commun. 2011;409(3):378–84.
50. Quan GM, Ojaimi J, Li Y, et al. Localization of pigment epithelium-derived factor in growing mouse bone. Calcif Tissue Int. 2005;76(2):146–53.
51. Broadhead ML, Akiyama T, Choong PF, Dass CR. The pathophysiological role of PEDF in bone diseases. Curr Mol Med. 2010;10(3):296–301.
52. Akiyama T, Dass CR, Shinoda Y, et al. PEDF regulates osteoclasts via osteoprotegerin and RANKL. Biochem Biophys Res Commun. 2010;391(1):789–94.